

1 **A single formula for the law of the wall and its application to wall-modelled**
2 **large-eddy simulation**

3 Fengshun Zhang (张风顺),^{1,2} Zhideng Zhou (周志登),^{1,3} Xiaolei Yang (杨晓雷),^{1,3, a)}
4 and Huan Zhang (张欢)²

5 ¹⁾*The State Key Laboratory of Nonlinear Mechanics, Institute of Mechanics,*
6 *Chinese Academy of Sciences, Beijing 100190, China*

7 ²⁾*Department of Mechanics and Engineering Science, Lanzhou University,*
8 *Lanzhou 730000, China*

9 ³⁾*School of Engineering Sciences, University of Chinese Academy of Sciences,*
10 *Beijing 100049, China*

11 (Dated: 20 April 2021)

12 In this work, we propose a single formula for the law of the wall, which is dubbed as
13 the logarithmic-exponential (LOG-EXP) formula, for predicting the mean velocity profile
14 in different regions near the wall. And then a feedforward neural network (FNN), whose
15 inputs and training data are based on this new formula, is trained for the wall-modelled
16 large-eddy simulation (WMLES) of turbulent channel flows. The direct numerical simula-
17 tion (DNS) data of turbulent channel flows is used to evaluate the performance of both the
18 formula and the FNN. Compared with the Werner-Wengle (WW) model for the WMLES,
19 a better performance of the FNN for the WMLES is observed for predicting the Reynolds
20 stresses.

^{a)}Electronic mail: xyang@imech.ac.cn

21 I. INTRODUCTION

22 The law of the wall is one of the cornerstones in wall-bounded turbulent flows^{1,2}. Different
 23 formulae have been proposed in the literature for the law of the wall. Roughly, they can be di-
 24 vided into two groups, i.e., the piecewise formulae and the single formulae. In the early year, the
 25 piecewise function was developed to describe the dynamics in different near-wall regions of the
 26 inner layer (e.g., for turbulent channel flows, it is located in the range of $0 \leq y \leq 0.1\delta$, where y
 27 denotes the wall-normal direction and δ is the half-height of the channel)³⁻¹⁰, which includes the
 28 viscous sublayer, the buffer layer and the logarithmic layer¹. The most widely used law of the wall
 29 describes the viscous sublayer using the linear profile, i.e.,

$$U^+ = y^+, \quad (1)$$

30 where $U^+ = U/u_\tau$, $y^+ = y/\delta_\nu$ with the friction velocity $u_\tau = \sqrt{\tau_w/\rho}$ (where τ_w is the wall shear
 31 stress and ρ is the fluid density) and the viscous scale $\delta_\nu = \nu/u_\tau$ (ν is the kinematic viscosity of
 32 the fluid), and the logarithmic layer using the logarithmic law, i.e.,

$$U^+ = \frac{1}{\kappa} \ln(y^+) + 5.0, \quad (2)$$

33 where $\kappa = 0.4$ is the Kármán constant. A list of different piecewise formulae proposed in the
 34 literature for the law of the wall is shown in Table I. There are two disadvantages of the piecewise
 35 formulae: 1) the velocity in the buffer layer is not accurately described; 2) the velocity derivative
 36 is discontinuous because of the piecewise nature of these formulae. To resolve these two issues,
 37 different types of the law of the wall based on single formula have been proposed in the litera-
 38 ture, which are often of two forms, i.e., the analytical form¹¹⁻¹⁶ and the numerical form^{17,18}. The
 39 analytical forms are usually complicated or do not have a sound prediction^{12,14-16}, while the nu-
 40 merical forms have a better prediction of the velocity profile^{17,18}, but do not have a clear physical
 41 meaning or difficult to use in practice. Different single formulae for the law of the wall proposed
 42 in the literature are shown in Table II and Table III.

44 In this work, we propose a new single formula named as the logarithmic-exponential (LOG-
 45 EXP) formula shown as follows:

$$U^+(y^+) = \frac{1}{\kappa} \ln(1 + \kappa y^+) + A \left(1 - e^{-\frac{y^+}{B}}\right) + C \left(1 - e^{-\frac{y^+}{D}}\right), \quad (3)$$

46 where $A = 11.630$, $B = 7.194$, $C = -4.472$ and $D = 2.766$, validate the proposed formula us-
 47 ing direct numerical simulation (DNS) data²⁸, the experimental data from other canonical wall

Authors	Formulae
Prandtl ³	$U^+ = y^+$ for $0 \leq y^+ \leq 11.5$
Taylor ⁴	$U^+ = 2.5 \ln(y^+) + 5.5$ for $11.5 \leq y^+$
Von Karman ⁵	$\begin{cases} U^+ = y^+, \text{ for } 0 \leq y^+ < 5 \\ U^+ = 5 \ln(y^+) - 3.05 \text{ for } 5 \leq y^+ < 30 \\ U^+ = 2.5 \ln(y^+) + 5.5 \text{ for } 30 \leq y^+ \end{cases}$
Deissler ⁶	$\begin{cases} U^+ = \int_0^{y^+} \left[1 + n^2 U^+ y^+ \left(1 - e^{-n^2 U^+ y^+} \right) \right]^{-1} dy^+, \text{ where } n = 0.124 \text{ for } 0 \leq y^+ < 26 \\ U^+ = 2.78 \ln(y^+) + 3.8, \text{ for } 26 \leq y^+ \end{cases}$
Rannie ⁷	$\begin{cases} U^+ = 1.454 \tanh(0.0688 y^+) \text{ for } 0 \leq y^+ < 27.5 \\ U^+ = 2.5 \ln(y^+) + 5.5 \text{ for } 27.5 \leq y^+ \end{cases}$
Breuer & Rodi ⁸	$\begin{cases} U^+ = y^+ \text{ for } 0 \leq y^+ < 5 \\ U^+ = A \ln(y^+) + B, \\ \quad \text{where } A = [k^{-1} \ln(30E) - 5] / \ln(6), B = 5 - A \ln(5) \text{ for } 5 \leq y^+ < 30 \\ U^+ = k^{-1} \ln(E y^+), \text{ where } E = 9.8 \text{ for } 30 \leq y^+ \end{cases}$
Werner & Wengle ⁹	$\begin{cases} U^+ = y^+ \text{ for } 0 \leq y^+ < 11.81 \\ U^+ = A (y^+)^B, \text{ where } A = 8.3, B = 1/7 \text{ for } 11.81 \leq y^+ \end{cases}$
Inagaki et al. ¹⁰	$\begin{cases} U^+ = y^+ \text{ for } 0 \leq y^+ < y_{C_1}^+ \\ U^+ = A_1 (y^+)^{B_1}, \text{ where } A_1 = 2.7, B_1 = 1/2, y_{C_1}^+ = A_1^{1/(1-B_1)} \text{ for } y_{C_1}^+ \leq y^+ < y_{C_2}^+ \\ U^+ = A_2 (y^+)^{B_2}, \text{ where } A_2 = 8.6, B_2 = 1/7, y_{C_2}^+ = (A_2/A_1)^{1/(B_1-B_2)} \text{ for } y_{C_2}^+ \leq y^+ \end{cases}$

TABLE I. Formulae for the law of the wall: piecewise function.

48 bounded flows^{29–31} and the classic law of the wall (i.e., Eq. (1) and Eq. (2)), and apply the new
49 single formula to wall-modelled large-eddy simulation (WMLES) via a feedforward neural net-
50 work (FNN) model for explicitly computing the wall shear stress using the wall-normal distance
51 and streamwise velocity.

52 The rest of this paper is organized as follows: in section II, the derivation process of the LOG-
53 EXP formula is presented; the proposed formula is validated using the DNS data of turbulent
54 channel flows and the experimental data of other canonical wall bounded flows in section III; then
55 it is applied WMLES via a feedforward neural network in section V; at last, conclusions are drawn

Authors	Formulae
Reichardt ¹¹	$U^+ = 2.5 \ln(1 + 0.4y^+) + 7.8 \left(1 - e^{-\frac{y^+}{11}} - \frac{y^+}{11} e^{-0.33y^+}\right)$
Spalding ¹²	$f(U^+) = U^+ + e^{-A} \left(e^{\kappa U^+} - 1 - \kappa U^+ - \frac{(\kappa U^+)^2}{2!} - \frac{(\kappa U^+)^3}{3!} - \frac{(\kappa U^+)^4}{4!}\right)$
Rasmussen ¹³	$y^+ = f(U^+)$, where $f(U^+) = U^+ + e^{-A} \left(2 \cosh(\kappa U^+) - (\kappa U^+)^2 - 2\right)$, $A = 2.2$, $\kappa = 0.4$
Musker ¹⁴	$U^+ = 5.424 \tan^{-1} \left[\frac{2y^+ - 8.15}{16.7}\right] + \log_{10} \left[\frac{(y^+ + 10.6)^{9.6}}{(y^+ - 8.15y^+ + 86)^2}\right] - 3.52 +$ $2.44 \left\{ \Pi \left[6 \left(\frac{y}{\delta}\right)^2 - 4 \left(\frac{y}{\delta}\right)^3\right] + \left[\left(\frac{y}{\delta}\right)^2 \left(1 - \frac{y}{\delta}\right)\right] \right\}$, $\Pi = 0.55$
Dean ¹⁵	$y^+ e^{\kappa g(\Pi, \frac{y}{\delta})} = f(U^+)$, $g(\Pi, \frac{y}{\delta}) = \frac{1}{\kappa} (1 + 6\Pi) \left(\frac{y}{\delta}\right)^2 - \frac{1}{\kappa} (1 + 4\Pi) \left(\frac{y}{\delta}\right)^3$ where $f(U^+)$ is given by Spalding or Rasmussen's expressions listed above
Monkewitz,	$U_{inner}^+ = U_{inner, 23}^+ + U_{inner, 25}^+$ $U_{inner, 23}^+ = 0.68285472 \ln(y^{+2} + 4.7673096y^+ + 9545.9963) +$ $1.2408249 \arctan(0.010238083y^+ + 0.024404056) +$ $1.2384572 \ln(y^+ + 95.232690) - 11.930683$
Chauhan and Nagib ¹⁶	$U_{inner, 25}^+ = -0.50435126 \ln(y^{+2} - 7.8796955y^+ + 78.389178) +$ $4.7413546 \arctan(0.12612158y^+ - 0.49689982)$ $-2.7768771 \ln(y^{+2} + 16.209175y^+ + 933.16587) +$ $0.37625729 \arctan(0.033952353y^+ + 0.27516982) +$ $6.5624567 \ln(y^+ + 13.670520) + 6.1128254$
van Driest ¹⁷	$U^+ = \int_0^{y^+} 2 \left[1 + \sqrt{1 + 0.64y^{+2} \left(1 - e^{-\frac{y^+}{26}}\right)^2}\right]^{-1} dy^+$
Duprat et al. ¹⁸	$\frac{\partial U^+}{\partial y^+} = \frac{\text{sign}(\frac{\partial P}{\partial x})(1 - \alpha)^{3/2} y^+ + \text{sign}(\tau_w) \alpha}{1 + \frac{y^+}{v}}$ $\frac{v}{v} = ky^+ \left[\alpha + y^+ (1 - \alpha)^{3/2}\right]^\beta \left(1 - e^{-y^+/(1 + A\alpha^3)}\right)^2$, where $\beta = 0.78$, $A = 17$, $\alpha = 1$
Cantwell ¹⁹	$U^+(y^+) = \int_0^{y^+} \left(-\frac{1}{2\lambda(s)^2} + \frac{1}{2\lambda(s)^2} \left(1 + 4\lambda(s)^2 \left(1 - \frac{s}{R\tau}\right)\right)^{1/2}\right) ds$ $\lambda(y^+) = \frac{\kappa y^+ (1 - e^{-(y^+/a)^m})}{\left(1 + \left(\frac{y^+}{bR\tau}\right)^n\right)^{1/n}}$, where $k = 0.4092$, $a = 20.095$, $m = 1.621$, $b = 0.3195$, $n = 1.619$.
Rotta ²⁰	$U^+ = \frac{1}{2\kappa I_m^+} \left(1 - \sqrt{1 + 4I_m^{+2}}\right) + \frac{1}{\kappa} \ln \left(2I_m^+ + \sqrt{1 + 4I_m^{+2}}\right) + \delta_l^+$, where $I_m = \kappa(y - \delta_l)$, $I_m^+ = u_\tau I_m / v$ and $\delta_l^+ = u_\tau \delta_l / v$ $\delta_l^+ = 5.0$ and experimental data ^{21,22} suggests $\delta_l^+ = 7.0$.

TABLE II. Formulae for the law of the wall: single formula.

Authors	Formulae
Nickels ²³	$U^+ = y_c^+ \left[1 - (1 + 2(y^+/y_c^+) + \frac{1}{2}(3 - p_x^+ y_c^+)(y^+/y_c^+)^2 - \frac{3}{2} p_x^+ y_c^+ (y^+/y_c^+)^3) e^{-3y^+/y_c^+} \right] +$ $\frac{\sqrt{1+p_x^+ y_c^+}}{6\kappa_0} \ln \left(\frac{1+(0.6(y^+/y_c^+))^6}{1+\eta^6} \right) + b \left(1 - e^{-\frac{5(\eta^4+\eta^8)}{1+5\eta^3}} \right), \text{ where } \eta = y/\delta, p_x^+ = (v/\rho U_\tau^3)/(dp/dx),$ $p_x^+ y_c^{+3} + y_c^{+2} - R_c^2 = 0, R_c = \frac{U_T y_c}{v} \text{ and } U_T = \sqrt{\tau(y = y_c)/\rho}$
Haritonidis ²⁴	$U^+ = \frac{1}{\lambda} \arctan \lambda y^+ - \frac{a}{2\lambda^2} \ln \left(1 + \lambda^2 y^{+2} \right), \text{ where } \lambda^2 = \alpha f^+, \alpha = \frac{nm^2}{2}, a = 1/h^+,$ <p>n is the number of ejections of equal strength, $f = 1/\Delta t_b$ is the bursting frequency,</p> $m = \kappa n^{-1} (\Delta t_e / \delta t_b)^{-1} \text{ and } \Delta t_e \text{ is the duration of the ejections.}$
Yakhot et al. ²⁵	$U^+(y^+) = \frac{1}{3\kappa} \left[4C^{1/4} - z + \ln \left(\frac{z+1}{z-1} \right) + 2 \arctan(z) - \ln \left(\frac{C^{1/4}+1}{C^{1/4}-1} \right) - 2 \arctan(C^{1/4}) \right],$ <p>where $z = (\hat{v}^3 - 1 + C)^{1/4} / \hat{v}^{3/4}$ and $\hat{v}^4 + (C-1)\hat{v} - \hat{v}_m^4 = 0$,</p> $\hat{v} = v_t/v, \hat{v}_m = \kappa l^+, l^+ = u_\tau l/v.$
Nikuradse ²⁶	$U^+ = \int_0^{y^+} 2 \left(1 - \frac{y^+}{Re_\tau} \right) \left[1 + \sqrt{1 + 4l_m^{+2} \left(1 - \frac{y^+}{Re_\tau} \right)} \right]^{-1} dy^+,$ $\frac{l_m}{\delta} = 0.14 - 0.08 \left(1 - \frac{y^+}{Re_\tau} \right)^2 - 0.06 \left(1 - \frac{y^+}{Re_\tau} \right)^4$
Cebeci, Bradshaw ²⁷	$U^+ = \int_0^{y^+} 2 \left(1 - \frac{y^+}{Re_\tau} \right) \left[1 + \sqrt{1 + 4l_m^{+2} \left(1 - \frac{y^+}{Re_\tau} \right)} \right]^{-1} dy^+,$ $\frac{l_m}{\delta} = \left(0.14 - 0.08 \left(1 - \frac{y^+}{Re_\tau} \right)^2 - 0.06 \left(1 - \frac{y^+}{Re_\tau} \right)^4 \right) \left(1 - e^{-\frac{y^+}{26}} \right)$

TABLE III. Formulae for the law of the wall: single formula.

56 in section V.

57 II. DERIVATION OF THE LOG-EXP FORMULA OF THE WALL

58 To derive the single formula for the law of the wall, we propose the following expression for
59 the first derivative of the mean streamwise velocity,

$$\frac{dU^+}{dy^+} = \frac{1}{1 + \kappa y^+} + \Phi(y^+) \quad (4)$$

60 where $\Phi(y^+)$ is the function to be given and satisfies these conditions, i.e., $\lim_{y^+ \rightarrow \infty} \Phi(y^+) =$
61 $\lim_{y^+ \rightarrow 0} \Phi(y^+) = 0$. It is noticed that this expression exactly satisfies the boundary condition at
62 the wall, i.e.,

$$\frac{dU^+}{dy^+} = 1 \text{ at } y^+ = 0, \quad (5)$$

63 and approximately satisfies the condition in the logarithmic layer, i.e.,

$$\frac{dU^+}{dy^+} = \frac{1}{\kappa y^+} \text{ for } y^+ \text{ in the logarithmic region,} \quad (6)$$

64 where y^+ is large enough such that the first term on the right-hand side of Eq. (4) can be approx-
 65 imated by $1/(\kappa y^+)$, and the second term on the right-hand side of Eq. (4) is considered being
 66 negligible.

67 There are many choices for $\Phi(y^+)$. In this work, we propose to use the following expression:

$$\Phi(y^+) = \frac{A}{B}e^{-\frac{y^+}{B}} + \frac{C}{D}e^{-\frac{y^+}{D}}, \quad (7)$$

68 where $A, B, C,$ and D are constants satisfying the following constraint

$$\frac{A}{B} + \frac{C}{D} = 0. \quad (8)$$

69 We will try to explain the physical meaning of the two exponential terms in Eq. (7) after we set
 70 the values of A, B, C and D . To obtain the law of the wall, we first substitute Eq. (7) into Eq. (4),
 71 which yields

$$\frac{dU^+}{dy^+} = \frac{1}{1 + \kappa y^+} + \frac{A}{B}e^{-\frac{y^+}{B}} + \frac{C}{D}e^{-\frac{y^+}{D}}. \quad (9)$$

72 Then, the expression for U^+ is obtained by integrating Eq. (9) with respect to y^+ as follows:

$$U^+(y^+) = \frac{1}{\kappa} \ln(1 + \kappa y^+) + A \left(1 - e^{-\frac{y^+}{B}}\right) + C \left(1 - e^{-\frac{y^+}{D}}\right). \quad (10)$$

73 Finally, the values of A, B, C and D are determined by fitting Eq. (10) using the DNS data²⁸ of the
 74 turbulent channel flow at $Re_\tau = 5200$ with the constraint shown in Eq. (8). Specifically, the mean
 75 velocity values in the range of $0 \leq y \leq 0.1\delta$ are employed to obtain the parameters as follows:
 76 $A = 11.630, B = 7.194, C = -4.472$ and $D = 2.766$.

77 We examine different terms in Eq. (9) in figure 1. As seen, the velocity derivative captured by
 78 the first term on the right-hand side of Eq. (9), i.e., $1/(1 + \kappa y^+)$, is less than the actual gradient.
 79 The second term on the right-hand side of Eq. (9), i.e., the exponential term with a positive co-
 80 efficient $(A/B)e^{-y^+/B}$, which increases as approaching the wall, takes into account the effect of
 81 increased turbulence as approaching the buffer layer region. The third term on the right-hand side
 82 of Eq. (9), i.e., the exponential term with a negative coefficient $(C/D)e^{-y^+/D}$, on the other hand,
 83 decreases as approaching the wall, which offsets the increase of the second term, and acts as a
 84 damping function in the near-wall region. It is noticed that we attempt to understand the effects of
 85 different terms in Eq. (9) instead of the exact physical interpretation of different terms.

87 The asymptotic behavior of the derived single formula is examined as follows. In the viscous
 88 sublayer, we expand Eq. (10) in Taylor series about $y^+ = 0$ and neglect the high order terms for

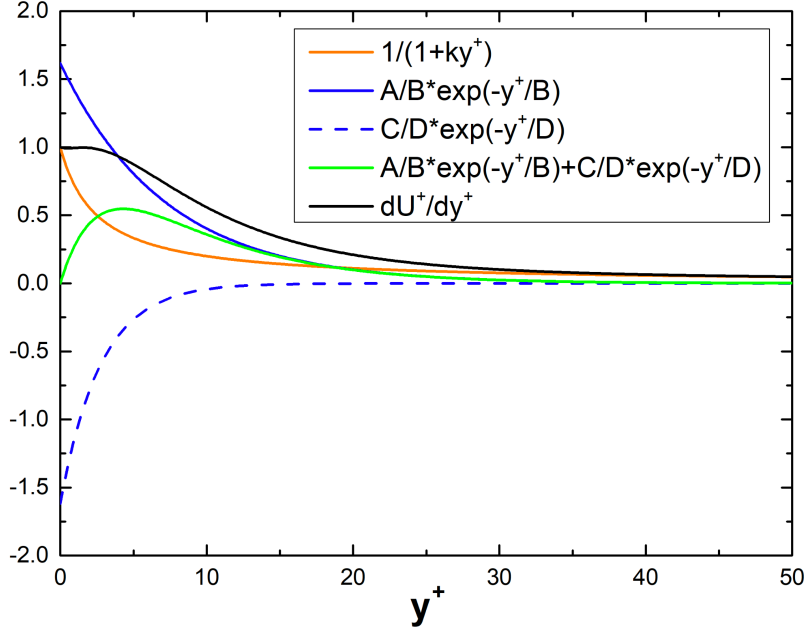


FIG. 1. Vertical variations of different terms in Eq. (10).

89 small y^+ and obtain the linear profile as follows:

$$\lim_{y^+ \rightarrow 0} U^+(y^+) \approx \lim_{y^+ \rightarrow 0} \left(y^+ + \frac{A}{B}y^+ + \frac{C}{D}y^+ \right) = y^+. \quad (11)$$

90 In the logarithmic region, where y^+ is large enough at high Reynolds numbers, the logarithmic
91 law can be recovered from Eq. (10) shown as follows:

$$\lim_{y^+ \rightarrow \infty} U^+(y^+) \approx \frac{1}{\kappa} \cdot \ln(y^+) + A - \frac{D \cdot A}{B} + \frac{\ln(\kappa)}{\kappa} = \frac{1}{\kappa} \ln(y^+) + 4.9 \quad (12)$$

92 considering that $\lim_{y^+ \rightarrow \infty} \ln(\kappa + y^+) \approx \ln(y^+)$ and $\lim_{y^+ \rightarrow \infty} e^{-\frac{y^+}{B}} \approx \lim_{y^+ \rightarrow \infty} e^{-\frac{y^+}{D}} \approx 0$.

93 III. VALIDATION OF THE LOG-EXP FORMULA

94 In this section we validate the proposed LOG-EXP formula, i.e., Eq. (10), using the DNS data
95 of turbulent channel flow²⁸, the experimental data from other canonical wall bounded flows^{29–31}.

96 Figure 2(a) compares the predictions from several single formulae with the DNS data at $Re_\tau =$
97 5200, which are employed for calibrating the proposed formula. It is shown that all the formulae
98 have a good prediction in the viscous sublayer and buffer layer. In the logarithmic region, which
99 is enlarged and shown in Figure 2(b), the predictions of the proposed LOG-EXP formula collapse
100 well with the DNS data, while some formulae, such as those predicted by Dean¹⁵, Reichardt¹¹,

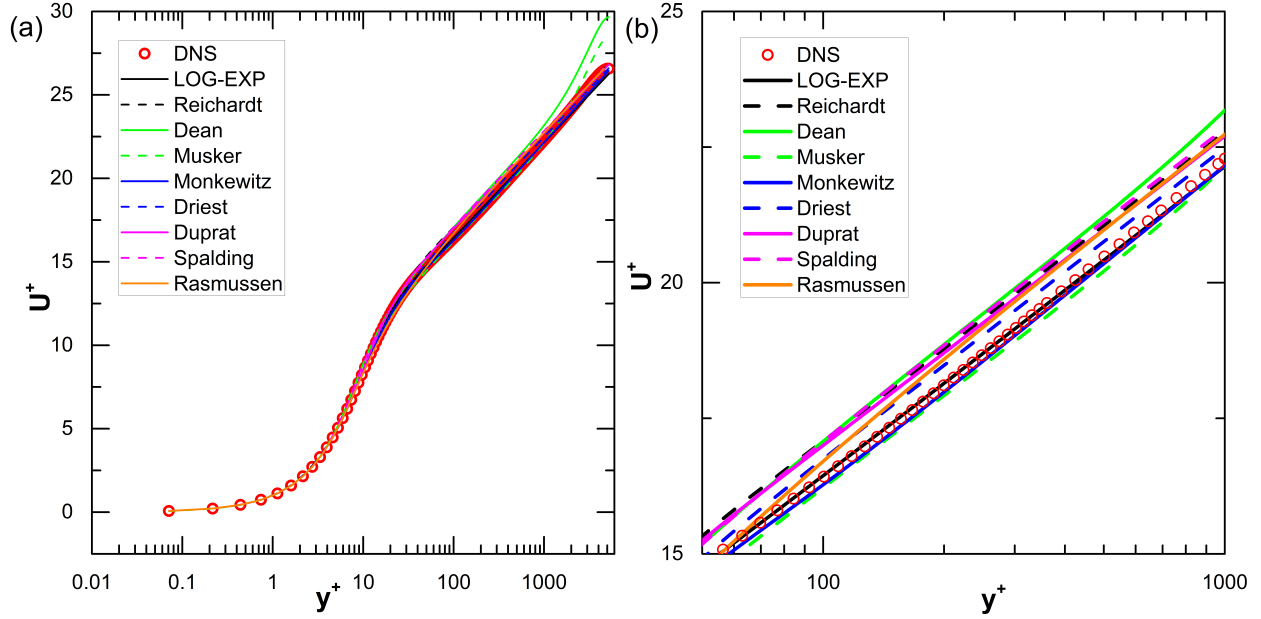


FIG. 2. (a) Comparison of the velocity profiles predicted by the LOG-EXP formula and others with that from DNS for the turbulent channel flow at Reynolds numbers $Re_\tau = 5200$ (b) Zoomed-in plot of (a) for $50 \leq y^+ \leq 1000$.

101 Spalding¹² and van Driest¹⁷, overpredict the velocity in this region. Furthermore, it is observed
 102 the predictions by Dean¹⁵ and Musker¹⁴ tend to deviate away from the DNS data. In Figure 3,
 103 we show the comparison of the first derivative of the velocity. As seen, predictions from different
 104 formulae agree well with the DNS data in the logarithmic layer and the outer layer. Discrepancies
 105 are observed in the viscous sublayer and buffer layer (i.e., $y^+ < 10$) for Reichardt's formula¹¹ and
 106 Dean's formula¹⁵, which overpredict the velocity derivative dU^+/dy^+ . The velocity derivative
 107 predicted by the proposed LOG-EXP formula, on the other hand, agrees well with DNS data for
 108 all vertical locations.

111 In Figure 4 and Figure 5, we compare predictions from the proposed LOG-EXP formula with
 112 the DNS data²⁸ for different Reynolds numbers. Although minor differences are observed for the
 113 low Reynolds number case with $Re_\tau = 180$, an overall good agreement is observed for both the
 114 velocity profile and the first derivative of dU^+/dy^+ for the proposed LOG-EXP formula.

117 To qualitatively evaluate the proposed LOG-EXP formula, we calculate the maximum absolute
 118 error of the velocity, which is defined by

$$e_{\max, U^+} = \max_{0 \leq \frac{y}{\delta} \leq 0.3} \frac{|U_F^+ - U_{DNS}^+|}{\langle |U_{DNS}^+| \rangle}, \quad (13)$$

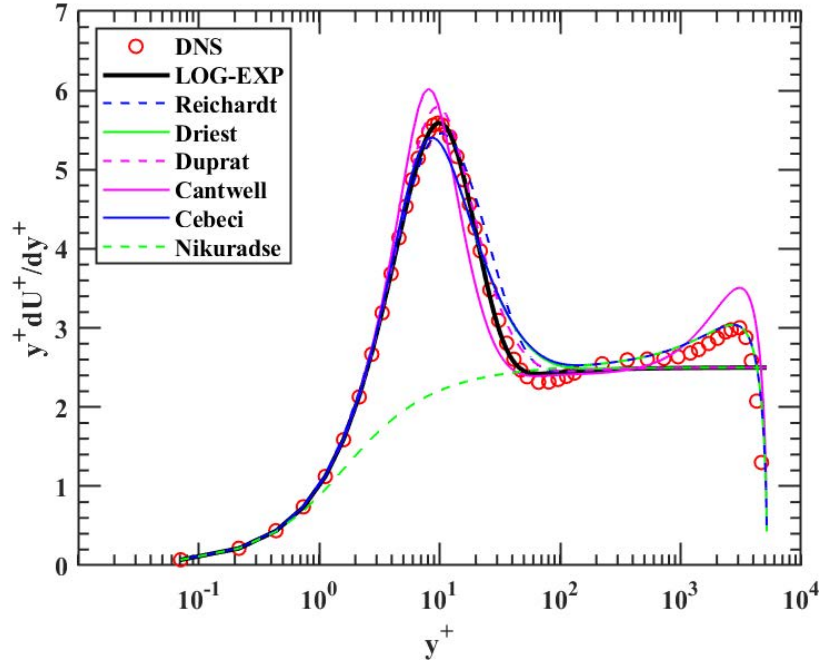


FIG. 3. Comparison of $y^+ dU^+/dy^+$ predicted by the LOG-EXP formula and others with that from DNS for the turbulent channel flow at Reynolds numbers $Re_\tau = 5200$.

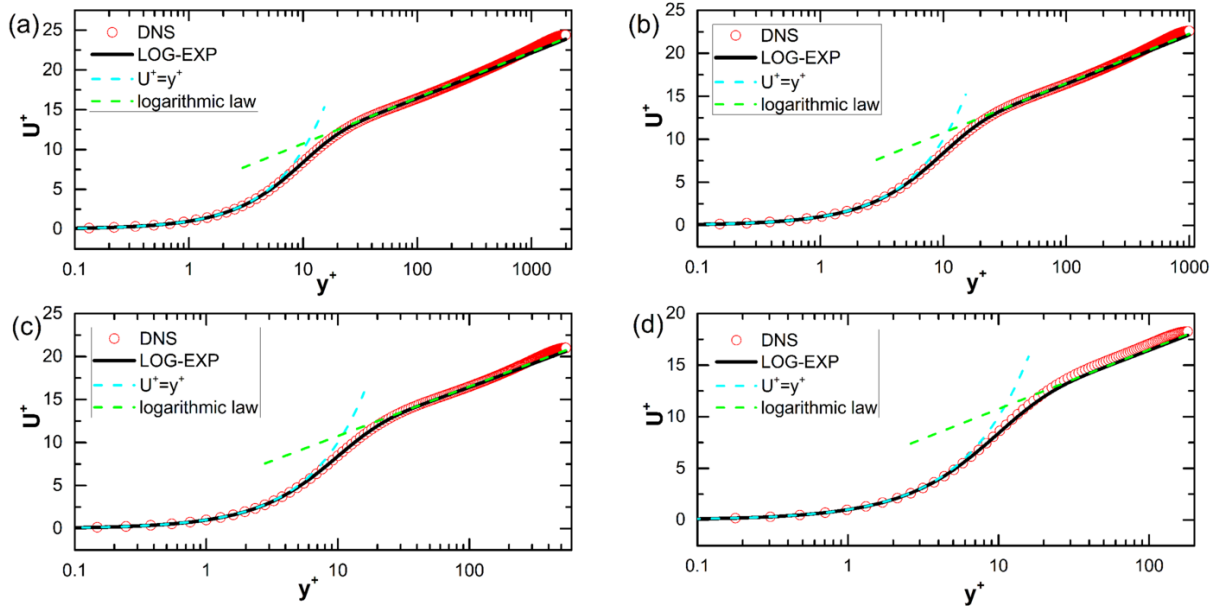


FIG. 4. Comparison of the velocity profiles predicted by the LOG-EXP formula with those from DNS for the turbulent channel flow with different Reynolds numbers for (a) $Re_\tau = 2000$, (b) $Re_\tau = 1000$, (c) $Re_\tau = 550$, and (d) $Re_\tau = 180$.

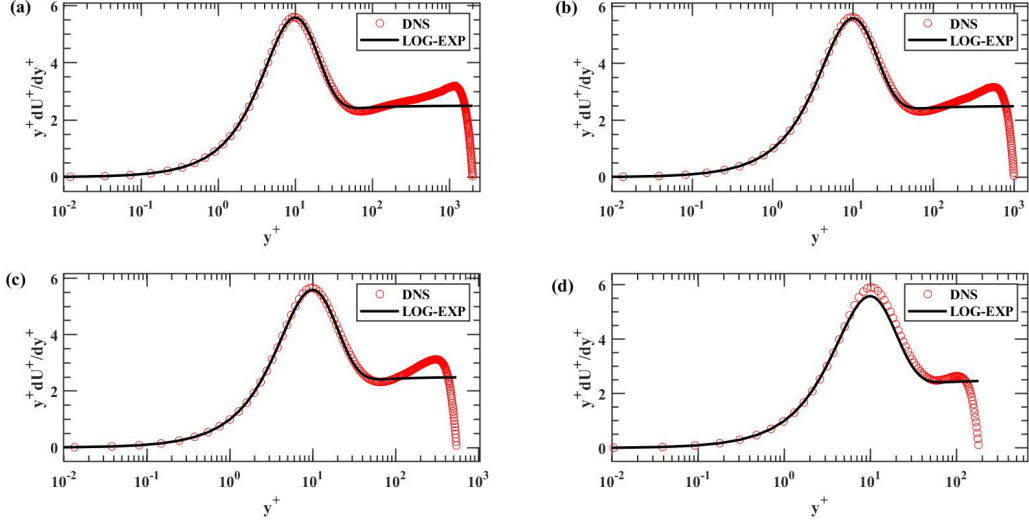


FIG. 5. Comparison of $y^+ dU^+/dy^+$ predicted by the LOG-EXP formula with those from DNS for the turbulent channel flow with different Reynolds numbers for (a) $Re_\tau = 2000$, (b) $Re_\tau = 1000$, (c) $Re_\tau = 550$, and (d) $Re_\tau = 180$.

119 where U_{DNS}^+ , U_F^+ and $\langle U_{DNS}^+ \rangle$ are the velocity of the DNS data, the velocity calculated by the
 120 single formula and the mean of U_{DNS}^+ averaged over $0.0 \leq y/\delta \leq 0.3$, and the maximum absolute
 121 error of dU^+/dy^+ , which is defined by

$$e_{\max, dU^+/dy^+} = \max_{0 \leq y/\delta \leq 0.3} \frac{\left| \left(\frac{dU^+}{dy^+} \right)_F - \left(\frac{dU^+}{dy^+} \right)_{DNS} \right|}{\left\langle \left| \left(\frac{dU^+}{dy^+} \right)_{DNS} \right| \right\rangle}, \quad (14)$$

122 where $(dU^+/dy^+)_{DNS}$, $(dU^+/dy^+)_F$ and $\langle (dU^+/dy^+)_{DNS} \rangle$ are the first derivative of the velocity
 123 of the DNS data, the first derivative of the velocity calculated from single formula and the mean
 124 value of $(dU^+/dy^+)_{DNS}$ averaged over $0.0 \leq y/\delta \leq 0.3$, respectively.

125 In Figure 6, we plot the errors of the velocity predicted by different formulae for different
 126 Reynolds numbers. As seen in Figure 6(a), the errors of the LOG-EXP predictions, which are
 127 less than 0.1, are lower than the other formulae except for the very low Reynolds number case.
 128 Figure 6(b) and (c) show the vertical location $y_{e_{\max, U^+}}$ where the e_{\max, U^+} occurs for different
 129 normalization, i.e., the viscous length scale δ_v and the channel half-height δ , respectively. It is
 130 observed that $y_{e_{\max, U^+}}$ increases with the increase of the Reynolds number when normalized using
 131 δ_v , while remains nearly constant for $y_{e_{\max, U^+}}$ when normalized using δ for the proposed LOG-
 132 EXP formula,

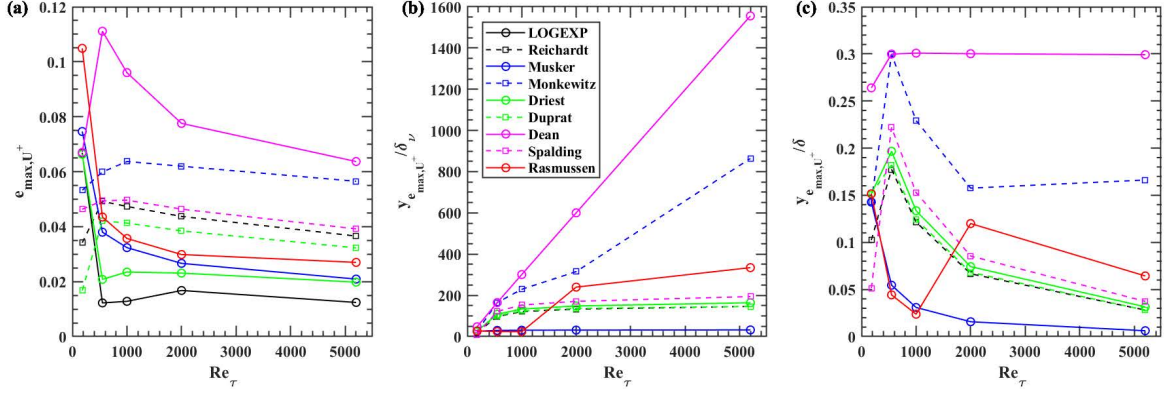


FIG. 6. (a) The maximum absolute error e_{\max, U^+} of the velocity predicted by different formulae compared with DNS data for different Reynolds numbers; (b) The vertical location in wall units $y_{e_{\max, U^+}} / \delta_\nu$ where the maximum absolute error occurs; (c) The vertical location normalized by the half-height of channel $y_{e_{\max, U^+}} / \delta$ where the maximum absolute error occurs.

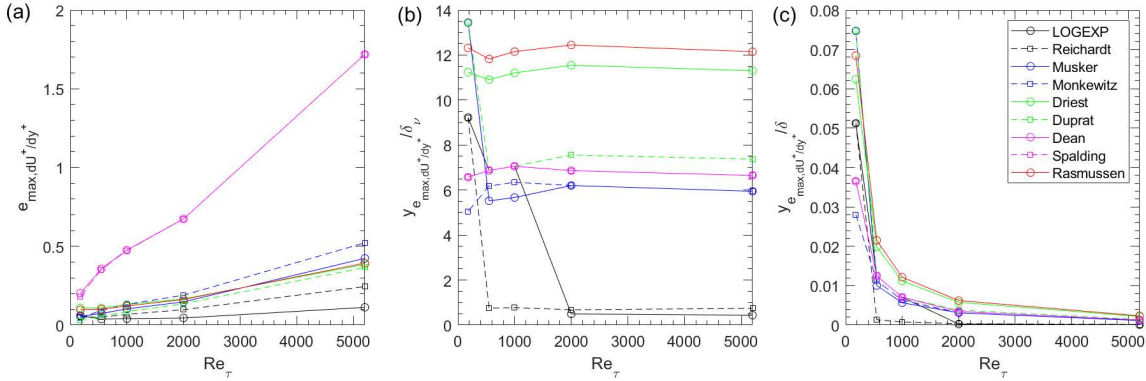


FIG. 7. Same as Figure 6 but for $e_{\max, dU^+/dy^+}$ and $y_{e_{\max, dU^+/dy^+}}$.

134 In Figure 7, the errors of the velocity derivatives predicted by different formulae are examined
 135 for different Reynolds numbers. As seen in Figure 7(a), the errors of the LOG-EXP predictions are
 136 lower than others, which increase via Reynolds number. Figure 7 (b) and (c) show the locations
 137 where the $e_{\max, dU^+/dy^+}$ occurs, which are normalized by the length scales δ_ν and δ , respectively.
 138 As seen, the $y_{e_{\max, dU^+/dy^+}}$ for velocity derivative is close to or within the viscous sublayer for differ-
 139 ent Reynolds numbers.

141 We further apply the proposed LOG-EXP formula to different types of canonical flows. Fig-
 142 ure 8 shows the semi-logarithmic plots of mean velocity profiles in the circular pipe flow^{29,31} and
 143 the turbulent boundary layer on a flat plate³⁰. An overall good agreement between the LOG-EXP

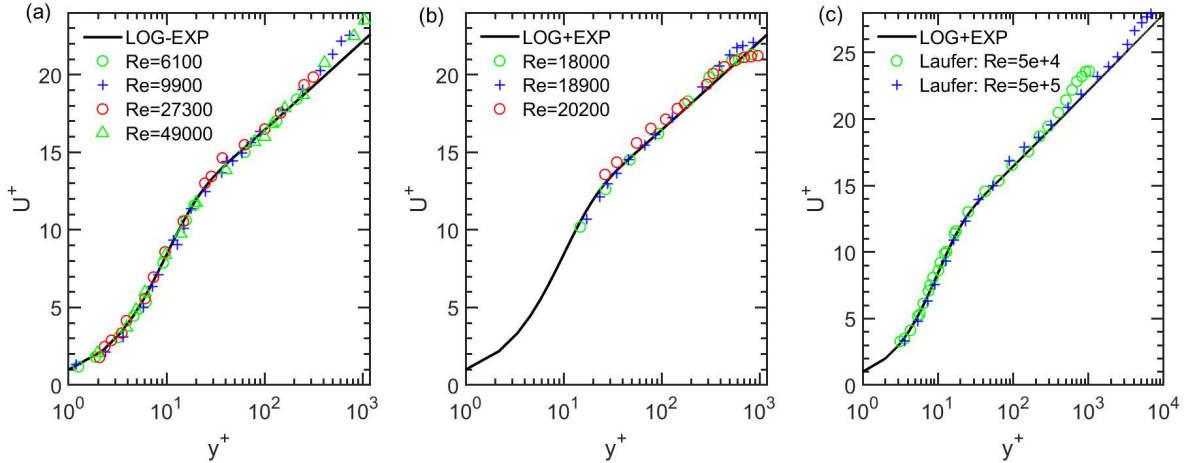


FIG. 8. Comparison of the velocity profiles predicted by the LOG-EXP formula with the experimental data from (a) Lindgren and Chao³¹, (b) Charnay et al.³⁰, (c) Laufer²⁹ for (a,c) the circular pipe flow and (b) the turbulent boundary layer on a flat plate.

148 formula and the experimental data is observed in the near wall region.

146 IV. APPLICATION OF THE LOG-EXP FORMULA TO WMLES

147 In this section, we apply the LOG-EXP formula to WMLES. In WMLES, the wall shear stress
 148 at the wall is often employed as approximate boundary conditions for outer flow simulations.
 149 However, the wall shear stress cannot be determined explicitly using the LOG-EXP formula. To
 150 address this issue, we employ the feedforward neural network (FNN) to construct an explicit LOG-
 151 EXP model for explicitly computing the wall shear stress (details on the model training and a priori
 152 test can be found in the appendix V. The explicit LOG-EXP model is then applied in WMLES and
 153 tested using turbulent channel flows at different Reynolds numbers.

154 The explicit LOG-EXP model is implemented in the large-eddy simulation module of the Vir-
 155 tual Flow Simulator (VFS-Wind) code^{32,33}. The governing equations are the incompressible
 156 Navier-Stokes equations, which are discretized spatially using the second-order central differenc-
 157 ing scheme, and advanced in time using a second-order fractional step method. The subgrid-scale
 158 stress is modeled using the dynamic procedure³⁴. In the implementation of the LOG-EXP wall
 159 model, the wall-tangential component of the velocity and wall-normal distance as the second off-
 160 wall grid nodes are employed as inputs for the LOG-EXP model, with computed wall shear stresses
 161 employed as boundary conditions for the outer flow simulation. For the wall-normal component

162 of the velocity, a no-slip boundary condition is employed.

163 Two cases with different Reynolds numbers are considered, i.e., the Reynolds number defined
164 using the friction velocity $Re_\tau = 1000, 5200$. For both cases, the computational domain is $L_x \times$
165 $L_y \times L_z = 7.0m \times 2.0m \times 3.5m$ in the streamwise, vertical and spanwise directions, respectively,
166 with the corresponding numbers of grid nodes $N_x \times N_y \times N_z = 33 \times 33 \times 33$, which are uniformly
167 distributed in all three directions.

168 We compare the predictions from WMLES with the LOG-EXP model with the DNS results³⁵
169 and those from the Werner-Wengle (WW) model⁹. It is shown in Figure 9 (a) that the mean velocity
170 profiles predicted by the WW model and the LOG-EXP model agree well with the DNS profile.
171 For the primary Reynolds shear stress $\langle u'v' \rangle^+$, figure 9 (b) shows that the WW model somewhat
172 overestimates the magnitude of $\langle u'v' \rangle^+$ for $200 < y^+ < 800$, which, on the other hand, is accurately
173 predicted by the LOG-EXP model. The comparisons of the normal Reynolds stresses are shown
174 in Figure 9 (c, d). It is observed that both wall models overpredict the streamwise component
175 of the normal Reynolds stress $\langle u'u' \rangle^+$, while underpredict the wall-normal component $\langle v'v' \rangle^+$.
176 Comparisons for the case with $Re_\tau = 5200$ are shown in Figure 10, with similar observations as
177 for the case with $Re_\tau = 1000$.

180 V. CONCLUSIONS

181 In this work, we proposed a new single formula for the law of the wall, which is dubbed as the
182 LOG-EXP formula. It is derived based on the decomposition of the velocity derivative into a term
183 satisfying the boundary conditions of the velocity derivative at the wall and in the logarithmic
184 region, and two exponential terms accounting for the increase of turbulence as approaching the
185 buffer layer and the viscous damping effect in the near-wall region, respectively. The derived
186 LOG-EXP formula, which is composed of a logarithmic term and two exponential terms, works
187 for the whole inner layer region and gives continuous predictions of both velocity and velocity
188 derivative. Its capability is evaluated using DNS data of turbulent channel flows and some other
189 canonical wall-bounded turbulent flows at different Reynolds numbers. Good agreements are
190 obtained for all the considered cases.

191 The proposed LOG-EXP formula is then applied to WMLES. To avoid the cost of solving the
192 LOG-EXP expression for the friction velocity, an explicit LOG-EXP model is developed using the
193 feedforward neural network for computing wall shear stress for WMLES. The WMLES with the

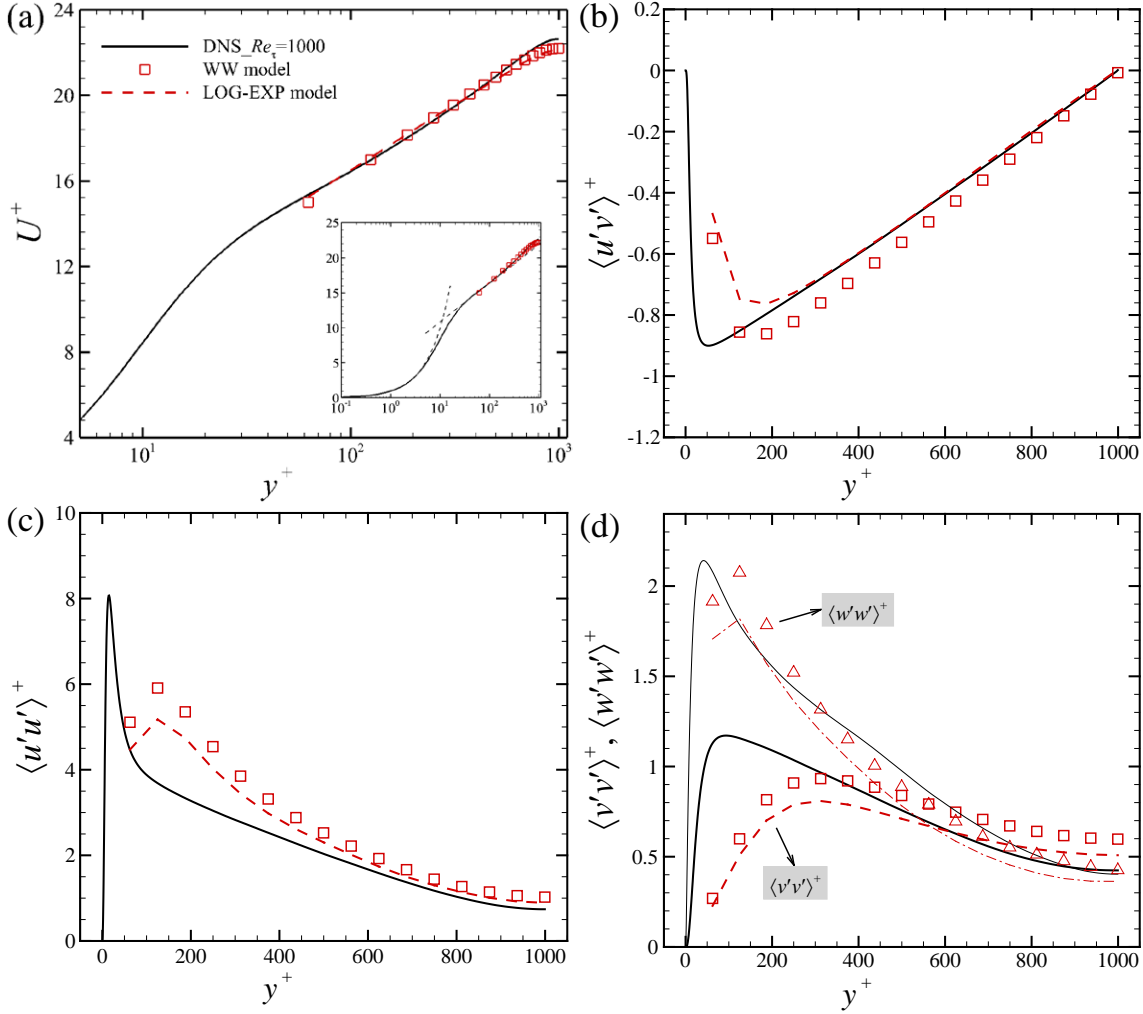


FIG. 9. Comparison of predictions from the WMLES with the LOG-EXP model with DNS and those from the WW model for (a) the mean streamwise velocity, (b) the primary Reynolds shear stress $\langle u'v' \rangle^+$, and (c, d) the normal Reynolds stresses $\langle u'u' \rangle^+$, $\langle v'v' \rangle^+$ and $\langle w'w' \rangle^+$, respectively.

194 LOG-EXP model is evaluated using the DNS data of turbulent channel flows. An overall good
 195 agreement is obtained for both mean streamwise velocity and the Reynolds stresses.

196 ACKNOWLEDGEMENTS

197 This work is partially supported by NSFC Basic Science Center Program for “Multiscale Prob-
 198 lems in Nonlinear Mechanics” (NO. 11988102).

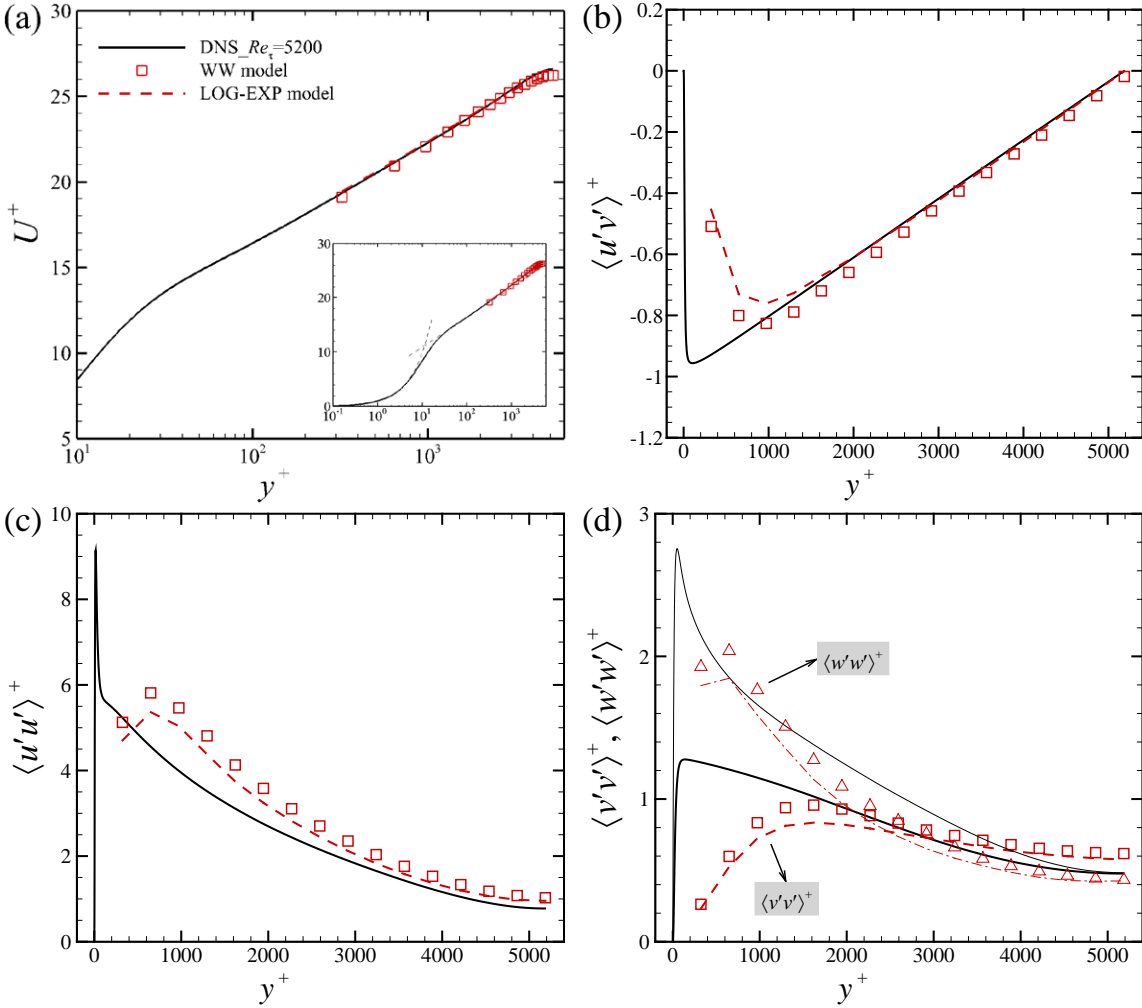


FIG. 10. The same as figure 9 but for $Re_\tau = 5200$.

199 **DATA AVAILABILITY**

200 The data that support the findings of this study are available from the corresponding author
 201 upon reasonable request.

202 **APPENDIX A: A NEURAL NETWORK MODEL FOR EXPLICITLY COMPUTING**
 203 **WALL SHEAR STRESS**

204 In this appendix, we describe the procedure for constructing a neural network model for explic-
 205 itly computing the wall shear stress using the wall-normal distance and the streamwise velocity,
 206 which can be used directly in WMLES without the need to solve the implicit LOG-EXP formula.

207 As shown in Figure 11, a multi-hidden-layer feedforward neural network is employed for the con-
 208 struction of the explicit model, which contains an input layer, multi hidden layers and an output
 209 layer. Each layer has a number of neurons, which are computational units that take weighted sums
 210 of the inputs to an activation function and calculate the output. Then the outputs of each layer are
 211 fed forward as inputs to the next layer. The training goal of the neural network is to find the op-
 212 timal weight and bias coefficients to minimize the loss of the neural network. More details about
 213 the neural network can be found in the reference³⁶.

214 The structure of the neural network employed in this work is shown in Tabel IV. The activation
 215 function used in this paper is the hyperbolic tangent function (tanh), which is defined as follows:

$$f(x) = \frac{e^x - e^{-x}}{e^x + e^{-x}}. \quad (15)$$

216 The input and output data are normalized using the Min-Max scaling,

$$x^* = \frac{x - x_{min}}{x_{max} - x_{min}}. \quad (16)$$

217 The loss function of the neural network is set as the mean square error (MSE), which is defined as
 218 follows:

$$L_{FNN} = \frac{1}{N_s} \sum_{i=1}^{N_s} (y_i - y_i^*)^2, \quad (17)$$

219 where N_s is the number of training samples, y_i and y_i^* are the FNN output and the labeled output
 220 from the training data, respectively. Besides, the error back-propagating (BP) scheme³⁷ and the
 222 Adam optimizer³⁸ are implemented with Keras³⁹ to train the FNN model.

223 The training data is obtained by solving the Eq. (3) about the friction velocity u_τ within the
 224 wall-normal distance in the range of $10^2 < y/\nu < 10^5$ and the streamwise velocity in the range of
 225 $0 < U < 1$. Data in $y^+ < 10$ are precluded because no wall model would be needed when the small
 226 scales are also resolved. Data above $y/\delta = 0.1$ are not included for training because the flow away
 227 from the wall is usually resolved by LES grids. Therefore, we have $10/u_\tau < y/\nu < 0.1Re_\tau/u_\tau$.
 228 For comparison purposes, we assume $u_\tau \approx 0.05$ and $0 < U < 1$, which are the same as the DNS
 229 data. Then we get the approximate range of y/ν . 501 points are selected evenly in the streamwise
 230 velocity range and 201 points are selected evenly in two adjacent orders of magnitude of y/ν , so
 231 that the training data contains about 501×603 input-output pairs. The neural network is trained
 232 to predict the friction velocity for given velocity and wall-normal distance. The inputs for training
 233 the neural network, which are defined based on the expression of the LOG-EXP formula as shown
 234 in Eq. 3, are shown in Table IV.

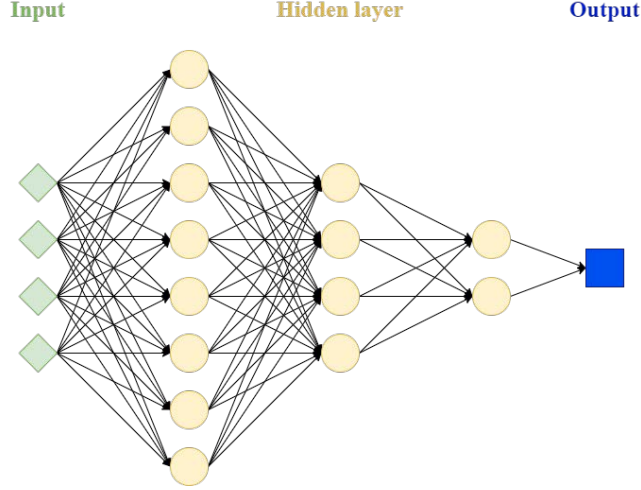


FIG. 11. Schematic diagram of the feedforward neural network (FNN) with multi hidden layers.

NN	AF	HL size	Input	Output
FNN	\tanh	(8,4,2)	$\frac{1}{k} \ln(1 + \frac{kyU}{v}), A(1 - e^{-\frac{yU}{vB}}), C(1 - e^{-\frac{yU}{vD}}), \sqrt{\frac{yU}{v}}$	$\frac{U}{u_\tau}$

TABLE IV. Details of the neural networks. Here NN denotes neural network, AF activation function and HL hidden layer. The tabulated hidden layer size contains the number of neurons within each hidden layer.

235 Figure 12 (a) shows the friction velocity predicted by the FNN model, as a function of the
 236 streamwise velocity and the wall-normal distance divided by the kinematic viscosity. As seen in
 237 Figure 12 (b), the relative error of the friction velocity, which is define by

$$u_{\tau RE} = \frac{|u_\tau - u_{\tau FNN}|}{u_\tau}, \quad (18)$$

238 where u_τ and $u_{\tau FNN}$ are calculated by Eq. 3 and FNN, respectively, is smaller than 0.5% for most
 239 cases. And the relative error of the velocity in wall units obtained by FNN is smaller than 1%,
 240 except for the case when the streamwise velocity is very small. Then we test the FNN model using
 241 the DNS data of turbulent channel flow with $Re_\tau = 1000^{35}$. As seen in Figure 13, the predictions
 242 from the FNN model fit well with the DNS data for different wall-normal distannces.

246 REFERENCES

247

248 ¹S. B. Pope, *Turbulent flows* (Cambridge University Press, Cambridge, 2001).

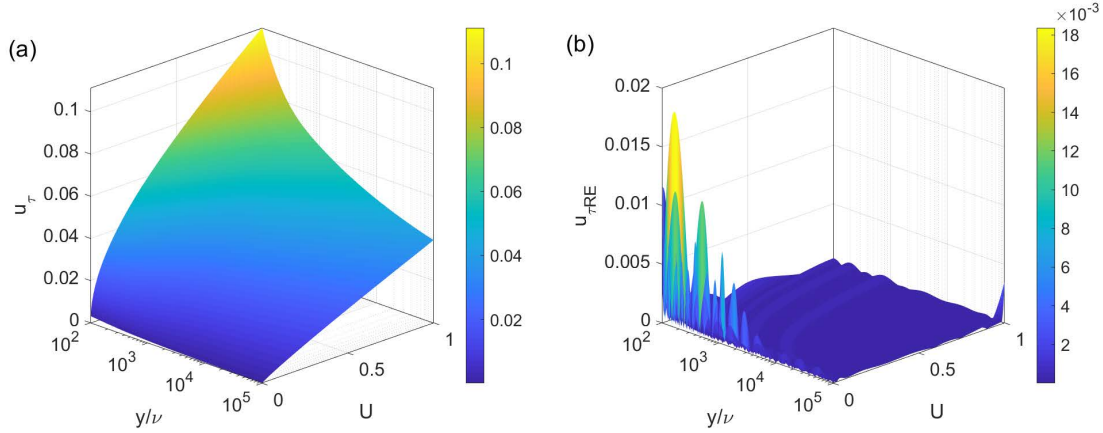


FIG. 12. Test of the FNN model using the data from the LOG-EXP formula for (a) the friction velocity and (b) relative error of the friction velocity predicted by FNN.

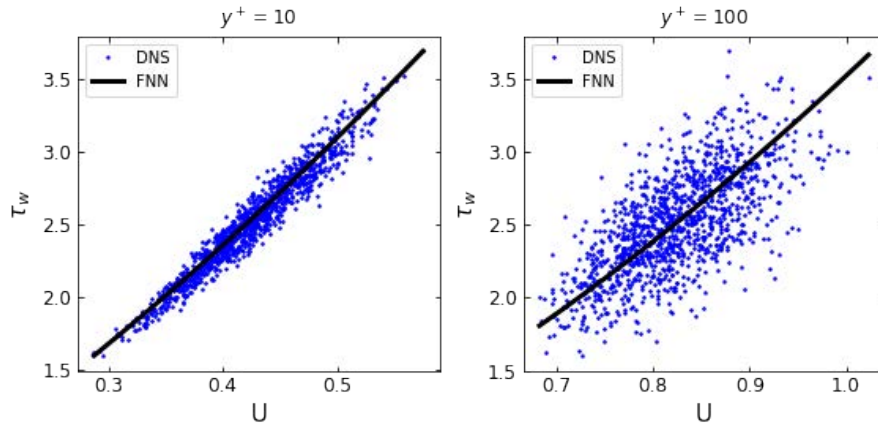


FIG. 13. Test of the FNN model using the DNS data of turbulence channel flow at $Re_\tau = 1000$ for (a) Wall shear stress as a function of the off-wall velocity at $y^+ \approx 10$ and (b) Wall shear stress as a function of the off-wall velocity at $y^+ \approx 100$.

249 ²P. A. Davidson, *Turbulence: an introduction for scientists and engineers* (Oxford university
250 press, 2015).

251 ³L. Prandtl, “Eine beziehung zwischen warmeaustausch und stromungswiderstand der flus-
252 sigkeiten,” *Phys. Z.* **11**, 1072–1078 (1910).

253 ⁴G. I. Taylor, “Conditions at the surface of a hot body exposed to the wind,” *Rep. Memo. of the*
254 *British Advisory Committee for Aeronautics* **272**, 423–429 (1916).

255 ⁵v. Kármán, “The analogy between fluid friction and heat transfer,” *Transactions of the American*
256 *Society of Mechanical Engineers* **61**, 705–710 (1939).

- 257 ⁶R. G. Deissler, *Analysis of turbulent heat transfer, mass transfer, and friction in smooth tubes at*
258 *high Prandtl and Schmidt numbers*, Vol. 1210 (National Advisory Committee for Aeronautics,
259 1954).
- 260 ⁷W. D. Rannie, "Heat transfer in turbulent shear flow," *Journal of the Aeronautical Sciences* **23**,
261 485–489 (1956).
- 262 ⁸M. Breuer and W. Rodi, "Large eddy simulation for complex turbulent flows of practical inter-
263 est," in *Flow simulation with high-performance computers II* (Springer, 1996) pp. 258–274.
- 264 ⁹H. Werner and H. Wengle, "Large-eddy simulation of turbulent flow over and around a cube in
265 a plate channel," in *Turbulent shear flows 8* (Springer, 1993) pp. 155–168.
- 266 ¹⁰M. Inagaki, O. Murata, T. Kondoh, and K. Abe, "Numerical prediction of fluid-resonant oscil-
267 lation at low mach number," *AIAA journal* **40**, 1823–1829 (2002).
- 268 ¹¹H. Reichardt, "Vollständige darstellung der turbulenten geschwindigkeitsverteilung in glatten
269 leitungen," *ZAMM-Journal of Applied Mathematics and Mechanics/Zeitschrift für Angewandte*
270 *Mathematik und Mechanik* **31**, 208–219 (1951).
- 271 ¹²D. B. Spalding, "A single formula for the "law of the wall"," *Transaction of the Asme Journal of*
272 *Applied Mechanics* **28**, 455 (1961).
- 273 ¹³M. Rasmussen, "On compressible turbulent boundary layers in the presence of favorable pres-
274 sure gradients," *American Society of Mechanical Engineers* (1975).
- 275 ¹⁴A. Musker, "Explicit expression for the smooth wall velocity distribution in a turbulent boundary
276 layer," *AIAA Journal* **17**, 655–657 (1979).
- 277 ¹⁵R. Dean, "A single formula for the complete velocity profile in a turbulent boundary layer,"
278 *Journal of Fluids Engineering* (1976).
- 279 ¹⁶P. A. Monkewitz, K. A. Chauhan, and H. M. Nagib, "Self-consistent high-reynolds-number
280 asymptotics for zero-pressure-gradient turbulent boundary layers," *Physics of Fluids* **19**, 115101
281 (2007).
- 282 ¹⁷E. R. Van Driest, "On turbulent flow near a wall," *Journal of the aeronautical sciences* **23**, 1007–
283 1011 (1956).
- 284 ¹⁸C. Duprat, G. Balarac, O. Métais, P. M. Congedo, and O. Brugière, "A wall-layer model for
285 large-eddy simulations of turbulent flows with/out pressure gradient," *Physics of Fluids* **23**,
286 015101 (2011).
- 287 ¹⁹B. J. Cantwell, "A universal velocity profile for smooth wall pipe flow," *Journal of Fluid Me-*
288 *chanics* **878**, 834–874 (2019).

- 289 ²⁰J. C. Rotta, “Das in wandnhe gültige geschwindigkeitsgesetz turbulenter strmungen,” *Ingenieur-*
290 *Archiv* **18**, 277–280 (1950).
- 291 ²¹P. Anderson, W. M. Kays, and R. J. Moffat, “The turbulent boundary layer on a porous plate: an
292 experimental study of the fluid mechanics for adverse free stream pressure gradients,” (1972).
- 293 ²²L. Purtell, P. Klebanoff, and F. Buckley, “Turbulent boundary layer at low reynolds number,”
294 *The Physics of Fluids* **24**, 802–811 (1981).
- 295 ²³NICKELS and B. T., “Inner scaling for wall-bounded flows subject to large pressure gradients,”
296 *Journal of Fluid Mechanics* **521**, 217–239 (2004).
- 297 ²⁴J. H. Haritonidis, “A model for near-wall turbulence,” *Physics of Fluids A Fluid Dynamics* **1**,
298 302–306 (1989).
- 299 ²⁵A. Yakhot, V. D. Khait, and S. A. Orszag, “Analytic expression for the universal logarithmic
300 velocity law,” *Journal of Fluids Engineering* **115** (1993).
- 301 ²⁶G. Nikuradse, “Laws of turbulent flow in smooth pipes,” (1966).
- 302 ²⁷T. Cebeci and P. Bradshaw, *Physical and Computational Aspects of Convective Heat Transfer*
303 (Springer-Verlag, 1984).
- 304 ²⁸M. Lee and R. D. Moser, “Direct numerical simulation of turbulent channel flow up to $Re_\tau \approx$
305 5200,” arXiv preprint arXiv:1410.7809 (2014).
- 306 ²⁹J. Laufer, “The structure of turbulence in fully developed pipe flow,” National Advisory Com-
307 mittee for Aeronautics Report (1953).
- 308 ³⁰G. Charnay, G. Comte-Bellot, and J. Mathieu, “Development of a turbulent boundary layer on a
309 flat plate in an external turbulent flow(effect of quasi-external isotropic turbulence on turbulent
310 boundary layer development on flat plate),” *AGARD Turbulent Shear Flows 9 p(SEE N 72-*
311 *20273 11-12)* (1972).
- 312 ³¹E. R. Lindgren and J. Chao, “Average velocity distribution of turbulent pipe flow with emphasis
313 on the viscous sublayer,” *The Physics of Fluids* **12**, 1364–1371 (1969).
- 314 ³²X. Yang, F. Sotiropoulos, R. J. Conzemius, J. N. Wachtler, and M. B. Strong, “Large-eddy
315 simulation of turbulent flow past wind turbines/farms: the virtual wind simulator (VWiS),” *Wind*
316 *Energy* **18**, 2025–2045 (2015).
- 317 ³³X. Yang and F. Sotiropoulos, “A new class of actuator surface models for wind turbines,” *Wind*
318 *Energy* **21**, 285–302 (2018).
- 319 ³⁴M. Germano, U. Piomelli, P. Moin, and W. H. Cabot, “A dynamic subgrid-scale eddy viscosity
320 model,” *Physics of Fluids A: Fluid Dynamics* **3**, 1760–1765 (1991).

- 321 ³⁵J. Graham, K. Kanov, X. Yang, M. Lee, N. Malaya, C. Lalescu, R. Burns, G. Eyink, A. Szalay,
322 R. Moser, *et al.*, “A web services accessible database of turbulent channel flow and its use for
323 testing a new integral wall model for les,” *Journal of Turbulence* **17**, 181–215 (2016).
- 324 ³⁶I. Goodfellow, Y. Bengio, A. Courville, and Y. Bengio, *Deep learning*, Vol. 1 (MIT press Cam-
325 bridge, 2016).
- 326 ³⁷D. E. Rumelhart, G. E. Hinton, and R. J. Williams, “Learning representations by back-
327 propagating errors,” *nature* **323**, 533–536 (1986).
- 328 ³⁸D. P. Kingma and J. Ba, “Adam: A method for stochastic optimization,” arXiv preprint
329 arXiv:1412.6980 (2014).
- 330 ³⁹F. Chollet, *Deep learning with Python*, Vol. 361 (Manning New York, 2018).